LAWRENCE
LIVERMORE
NATIONAL
LABORATORY

UCRL-CONF-206035

Adaptive compensation of atmospheric turbulence utilizing an interferometric wave-front sensor and a high-resolution MEMS-based spatial light modulator

Kevin Baker, Eddy Stappaerts, Don Gavel, Jack Tucker, Dennis Silva, Scott Wilks, Scot Olivier, Jeff Olsen

August 13, 2004

SPIE
Denver, CO, United States
August 2, 2004 through August 6, 2004

Adaptive compensation of atmospheric turbulence utilizing an interferometric wave-front sensor and a high-resolution MEMS-based spatial light modulator

K.L. Baker, E.A. Stappaerts, D. Gavel, J. Tucker, D.A. Silva, S.C. Wilks, S.S. Olivier, J. Olsen

Lawrence Livermore National Laboratory, Livermore, CA, USA

Abstract

Horizontal path correction of optical beam propagation presents a severe challenge to adaptive optics systems due to the short transverse coherence length and the high degree of scintillation incurred by propagation along these paths. The system presented operates with nearly monochromatic light. It does not require a global reconstruction of the phase, thereby eliminating issues with branch points and making its performance relatively unaffected by scintillation. The systems pixel count, 1024, and relatively high correction speed, in excess of 800 Hz, enable its use for correction of horizontal path beam propagation. We present results from laboratory and field tests of the system in which we have achieved Strehl ratios greater than 0.5.

keywords: Adaptive, Optics

I. INTRODUCTION

Adaptive optics (AO) systems used in astronomy and vision applications typically utilize Shack-Hartmann wave-front sensors.[1,2] These sensors measure the gradient of the phase and commonly utilize least squares phase reconstruction algorithms. When coherent light propagates over atmospheric paths, the beam develops large intensity fluctuations and phase residues,[3] severely degrading the performance of these wave-front sensors. Recently, a prototype of the coherent light AO system described in this article was demonstrated using a visible laser and a liquid crystal spatial light modulator (SLM).[6] It allowed many concept features to be tested, but its speed was limited to ~1 Hz due to the SLM response time. This article discusses a coherent light AO system based on a quadrature Twyman-Green interferometer operating at a wavelength of 1.5 μm and at speeds in excess of 800 Hz through atmospheric turbulence.[5,6] The technique mixes an atmospheric probe beam with a large amplitude reference beam, allowing it operate in a photon-noise limited regime even in the case of large scintillation. It does not require a global reconstruction of the phase, making it much less sensitive to phase residues.[7] These attributes make this approach to phase conjugation much more robust than conventional AO systems employing Shack-Hartmann wave-front sensors, for applications involving coherent light propagation through strong turbulence.

In section II, the experimental layout of the phase conjugate engine is presented along with a description of its operation. Section III details the experimental characterization and operation of the system with Kolmogorov phase screens in a laboratory setting. Section IV details the experimental characterization and operation of the system in a field test with atmospheric turbulence. These results are then summarized in the V and final section.

II. EXPERIMENTAL LAYOUT

The optical layout of the IR laboratory breadboard system is shown in Figure 1. It consists primarily of an interferometric wave-front sensor, a MEMS-based spatial-light-modulator built by the Boston Micromachines Corporation (BMC), an Erbium-doped fiber laser built by HRL laboratories and computer hardware/software to analyze the wave-front and implement the phase correction. The system was designed for open-loop operation, however, a closed-loop arm exists such that the wave-front camera can be aligned precisely with the MEMS-based spatial light modulator and either configuration can be used

simply by blocking the remaining beam path. The laser source is an Erbium-doped fiber laser operating at 1530 nm. The laser has two independently triggerable arms, which output nearly transform-limited pulses of 1 ns duration and pulse energies of 7 μJ and 100 nJ for the probe beam and the reference beam, respectively.

Polarization components are utilized in the testbed to form the two interferograms with a $\pi/2$ phase shift between them and also to control the relative signal levels in the arms of the interferometer. The reference beam passes through a quarter waveplate converting the linearly polarized light into circularly polarized light. The reference beam is mixed with the probe beam after the probe beam has traversed the aberrating medium, atmosphere or Kolmogorov phase screens, and passed through a half waveplate to rotate the polarization such that equal components of horizontal and vertical fields in the probe beam are combined with the circularly polarized reference beam. A wollaston prism is then used to angularly separate the horizontal and vertical polarizations of the reference and probe beams into the two interferograms with a $\pi/2$ phase shift between the reference beams in the two separate interferograms.

III. LABORATORY EXPERIMENTAL RESULTS

The ability of the phase conjugate engine to correct phase aberrations was initially tested in the laboratory using three phase plates to represent the atmospherically induced aberrations. The phase plates were designed to produce a Kolmogorov turbulence spectrum, thereby simulating atmospheric propagation. In order to test the system performance, the phase plates were first characterized on the IR system after fabrication. Once the phase plate characterization was complete, a quantitative analysis of the phase conjugate engine was performed. The phase plates were mounted on a common axis such that the plates could be rotated transverse to the optical axis to simulate transverse wind velocity and to test the temporal performance of the phase conjugate engine.

The plates were first characterized by measuring the aberrated phase profile passing through the phase plates and subsequently unwrapping the phase. This task was accomplished by taking a large number of interferograms, ~3000, as the phase plates were rotated. The interferograms allowed the determination of the two-dimensional wrapped (modulo-2π) phase across the input aperture of the system. Before the

parameters used to describe the turbulence spectrum could be determined, the phase had to be unwrapped. The phase was unwrapped using a minimum weighted discontinuity method.[7] This technique partitions the wrapped phase profile into two connected regions, separated by discontinuity curves. The algorithm then raises the phase in one of the regions by 2π, thereby reducing the weighted sum of the discontinuities. This process is repeated until no further partitioning is possible. Once the unwrapped phase has been recovered, the parameters and scaling relations used to describe the turbulence spectrum can be determined. One such scaling relation is the phase structure function, $D_\phi(r)$. The phase structure function is defined by $D_\phi(r) = <|\bullet\phi(x)-\bullet\phi(x+r)|^2>$, which for a Kolmogorov turbulence spectrum can be expressed analytically as $D_\phi(r) = 6.88(r/r_o)^{5/3}$, in the limit $r>>(\lambda L)^{0.5}$. In this expression, r_o is the Fried parameter or transverse coherence length and λ and L are the wavelength and propagation length, respectively.[8] The phase structure function is constructed by comparing the phase at a given location to the phase at an increasing distance from that location. A median average over 3000 such structure functions, collected while the plates were rotating, is shown in Figure 2. Again there is a close fit between the slopes of the experimentally averaged structure functions and the analytic structure function expected from a Kolmogorov turbulence spectrum. In this case, the solid black line represents the experimentally measured data and the solid and dashed gray lines represents analytic Kolmogorov fits for a Fried parameter of 1.0 mm and 1.3 mm, respectively.

Once the phase plates were characterized, then the system performance was quantified, primarily by determining the Strehl ratio. The Strehl ratio was calculated by measuring both the point-spread-function (PSF) with a far-field camera and the near-field image of the probe beam with the wave-front camera. With these two measurements, the Strehl ratio was calculated and compared with the expected phase variances associated with a Kolmogorov turbulence spectrum. The near-field image of the probe beam after transmission through the phase plates was measured at the wave-front camera, which is in a conjugate image plane to the input aperture of the system. The near-field image was taken by temporarily blocking the reference beam. Using the far-field camera, the PSF was recorded as the adaptive optics system was measuring the wave-front. Fig. 3 shows the PSF for the uncorrected probe beam, Fig. 3a, and the corrected probe beam, Fig. 3b. With these two measurements, the Strehl ratio was calculated and compared with the expected phase variance associated with a Kolmogorov turbulence spectrum.

The instantaneous Strehl ratios corresponding to the measured PSF's were averaged over 100

separate frames to examine the fitting error associated with the adaptive optics system. The resultant averaged Strehl ratio in this case was S_r=0.55 at the slowest phase plate speed of v=0.75 cm/sec. The strehl ratio due to the fitting error for a Kolmogorov turbulence spectrum is given by the expression $S_r=\exp\{-1.3(d/r_o)^{5/3}\}$, for a square aperture, where d is the sub-aperture size.[9] For the laboratory demonstration, the sub-aperture size is approximately 11.4/32 or 356 μm. The expected Strehl ratio from fitting error in this case would be $S_r \sim 0.84$, which is slightly higher than the measured Strehl ratio of S_r=0.55. The MEMS-based spatial light modulator, which consisted of 32x32 pixels, in the phase conjugate engine had approximately 60 bad pixels and the outer actuators were not activated giving nearly 18% of the actuators that were not contributing to the correction. Wave optics simulations performed using a bad pixel map of the actuators indicated that the non-activated pixels caused a reduction in the Strehl ratio of approximately 22 %. This gave an estimated maximum Strehl achievable of approximately $S_r=(1.0-0.22)*\exp\{-1.3(d/r_o)^{5/3}\}$ or S_r~0.66. The maximum achievable Strehl is also reduced by the 3-bit algorithm[10,11] used to determine the phase which lowers the Strehl ratio by an additional factor of 0.95 to S_r~0.95*0.66 = 0.63, which is within approximately 15 % of the measured average Strehl ratio.

The instantaneous Strehl ratios can then be averaged over the 100 separate frames for each of the velocities to examine the time delay error associated with the adaptive optics system. The time delay error arises because of the finite time between measurement of the aberrated wave-front and application of the correction to the MEMS device. During this time delay, the high frequency components of the atmosphere undergo a significant change and the system is unable to correct the highest turbulence frequencies. The time delay, τ, is the time between when the probe beam samples the atmosphere and when the correction has been applied to the spatial light modulator, which in the case of the adaptive optics system was generally 1/580 hz or 1.72 ms. The resultant averaged Strehl ratio for each of the transverse plate velocities is displayed as the black line in Figure 4. This experimentally determined Strehl ratio was then fit to the analytical Strehl ratio for a Kolmogorov turbulence spectrum, $\exp\{-6.88(v\tau/r_o)^{5/3}\}$, normalized to the Strehl ratio obtained when the phase plates are stationary. A fit with r_o=1.1 mm was achieved, again in agreement with the previous measurements.

IV. FIELD TEST EXPERIMENTAL RESULTS

The topology of the field test site was defined by rolling hills. The experiment was carried out across a valley between two of these hills, one of which contained the AO system and the other a 2-mirror retro-reflector. The AO system was slightly higher in elevation than the retro-reflector, with an approximate drop in elevation of 100 meters to the valley floor between the two hills. The roundtrip distance traveled by the probe beam was approximately 1.35 km, for a transit time of approximately 4.5 μs.

The turbulence over the propagation path was characterized by measuring the aberrated phase profile of the probe beam after passing through the atmosphere. A large number of interferograms, ~3000, were acquired at a frequency of ~580 Hz. These interferograms contained the information required to determine the two-dimensional, wrapped (modulo-2π), phase across the input aperture of the system. Before the parameters used to describe the turbulence spectrum could be determined, the phase was unwrapped using a minimum weighted discontinuity method as discussed in section III.[7] The phase structure function is constructed by comparing the phase at a given location to the phase at an increasing distance from that location. An average over 3000 such functions is shown in Fig. 5. There is a good fit between the slopes of the averaged, experimentally determined, function and the analytic form for a Kolmogorov turbulence spectrum. The solid black line represents the data, the solid gray line represents the Kolmogorov fit for a Fried parameter of 2.4 cm and the two dashed black lines represent Kolmogorov fits for Fried parameters of 2.0 cm and 3.0 cm, respectively.

The performance of the AO system was again quantified by measuring the Strehl ratio. The Strehl ratio was calculated by measuring both the point-spread-function (PSF), with a far-field camera, and the near-field image of the probe beam, with the wave-front camera. The near field images were collected at a slightly delayed time by blocking the reference beam. Fig. 6 shows the PSF for the uncorrected probe beam, Fig. 6a, and the corrected probe beam, Fig. 6b. With these two measurements, the Strehl ratio was calculated and compared with the expected phase variance associated with a Kolmogorov turbulence spectrum. A sequence of 100 PSFs was taken and the absolute instantaneous Strehl ratios determined from these measurements, with the system on and off, as shown in Fig. 7. The instantaneous Strehl ratios were averaged over the 100 frames to quantify the system performance. The figure indicates an average corrected Strehl ratio of S_r=0.46, a tip/tilt only Strehl ratio of S_r=0.19 and a Strehl ratio of S_r=0.06 without

tip/tilt correction. The uncorrected value, S_r=0.06, is in reasonably good agreement with the expected value of $S_r=(r_o/D)^2=(2.4\text{ cm}/13\text{ cm})^2=0.03$.

An estimate of the Strehl ratio with the system on was made as follows. The ratio due to the fitting error, for a Kolmogorov turbulence spectrum and a square aperture, is given by $S_r=\exp\{-1.3(d/r_o)^{5/3}\}$, where d is the sub-aperture size.[9] For the field test, the sub-aperture size was approximately 4 mm, yielding an expected Strehl ratio of Sr ~ 0.94.. As discussed in section III, simulations performed taking the bad pixels in the SLM into account indicated a reduction in the Strehl ratio of approximately 22%, giving an estimated maximum achievable Strehl ratio of $S_r=(1.0\text{-}0.22)\exp\{-1.3(d/r_o)^{5/3}\}\sim0.73$. Given the wind velocities and system operating speeds, the effects of time delay error were negligible. The achievable Strehl ratio is further reduced by the 3-bit algorithm used to determine the phase, lowering it by a factor of 0.95 to $S_r\sim0.95*0.73 = 0.69$.[10,11] The measured value of 0.46 is then within approximately 40 % of the maximum achievable Strehl ratio. The discrepancy is likely due to slight registration errors, camera gain nonlinearities and small errors in calibration of the SLM response curves.

V. SUMMARY

In the laboratory, the phase conjugate engine achieved large improvements over the uncorrected, non-tip-tilt corrected PSF resulting from propagation through the phase plates. This can be seen in Figure 3 which displays the measured point-spread-function for the adaptive optics system when the system is uncorrected and corrected, respectively. Figure 4 indicates a corrected average Strehl ratio of S_r=0.55 at the slowest phase plate speed of v=0.75 cm/sec and an uncorrected Strehl ratio of S_r=0.01 without tip/tilt correction. The measured uncorrected Strehl ratio of S_r=0.01 is in agreement with the expected Strehl ratio of $S_r=(r_o/D)^2=(1.2\text{ mm}/11.4\text{ mm})^2=0.011$.

In the field test, the AO system achieved large improvements, ~8x, over the uncorrected PSF. The system successfully demonstrated the use of a large actuator number, 1024, MEMS-based SLM at speeds in excess of 800 Hz. This work demonstrates the potential of such SLMs to replace conventional deformable mirrors for applications requiring high Strehl ratios such as multi-conjugate and extreme AO systems, AO systems for extremely large telescopes and communications and imaging under conditions of strong turbulence.

Acknowledgements

The authors would like to acknowledge M.L. Minden and Hughes Research Laboratories for providing the Erbium-doped fiber laser used in these experiments. The authors would also like to acknowledge P. Bierden and the Boston Research Corporation for providing the MEMS-based spatial light modulator. The authors would also like to acknowledge discussions with W.H Long, Jr. regarding simulations of the expected performance of the system in various applications. The authors would like to acknowledge H. Komine for suggesting a Wollaston prism, in the configuration shown in Figure 1, for channel separation on the CCD camera and L.G. Seppala for contributions to the optical design. This effort was sponsored by the Defense Advanced Research Projects Agency (DARPA) for work on the Coherent Communications, Imaging and Targeting (CCIT) program, 02-L493. This work was performed under the auspices of the U.S. Department of Energy by the University of California, Lawrence Livermore National Laboratory under contract No. W-7405-Eng-48.

REFERENCES

[1] J. W. Hardy, *Adaptive Optics for Astronomical Telescopes* (Oxford University Press, Oxford, 1998).

[2] R. K. Tyson, *Principles of Adaptive Optics* (Academic Press, Boston, 1998).

[3] R. Dou and M. K. Giles, "Closed-loop adaptive-optics system with a liquid-crystal television as a phase retarder," Opt. Lett. **20**, 1583 (1995).

[4] T. Shirai, T. H. Barnes, and T. G. Haskell, "Adaptive wave-front correction by means of all-optical feedback interferometry," Opt. Lett. **25**, 773 (2000).

[5] K. L. Baker, E. A. Stappaerts, S. C. Wilks, P.E. Young, D. Gavel, J. Tucker, D.A. Silva and S.S. Olivier, "Open and Closed-Loop Aberration Correction using a Quadrature Interferometric Wave-Front Sensor," Opt. Lett. **29**, 47 (2004).

[6] C. J. Buchenauer and A. R. Jacobson, "Quadrature Interferometer for plasma density measurements," Rev. Sci. Instrum. **48**, 769 (1977).

[7] T. J. Flynn, "Two-dimensional phase unwrapping with minimum weighted discontinuity," JOSA A **14**, 2692 (1997).

[8] D.L. Fried "Optical resolution through a randomly inhomogeneous medium for very long and very short exposures," JOSA Vol.56 No.10 pp1372-1379 (1966).

[9] R. Hudgin, "Wave-front compensation error due to finite corrector-element size," JOSA Vol.67 No.3, pp393-395 (1977).

[10] Gordon D. Love, Nigel Andrews, Philip Burch, David Buscher, Peter Doel, Colin Dunlop, John Major, Richard Myers, Alan Purvis, Ray Sharples, Andrew Vick, Andrew Zadrozny, Sergio R. Restaino and Andreas Glindemann, "Binary adaptive optics: atmospheric wave-front correction with a half-wave phase shifter," Applied Optics **34**, 6058 (1995).

[11] K. L. Baker, E. A. Stappaerts, S. C. Wilks, D. Gavel, P.E. Young, J. Tucker, D.A. Silva, S.S. Olivier and J. Olsen, "Performance of a phase-conjugate-engine implementing a finite-bit phase correction," Opt. Lett. **29**, pp980-982 (2004).

FIGURE CAPTIONS

Figure 1 Laboratory breadboard setup used to test the performance of the phase conjugate engine in a controlled laboratory environment. The abbreviations stand for the following: BS, beam splitters; M, mirrors; L, lenses; S, shutters; A, apertures; TFP, thin film polarizers; λ/2 and λ /4, half and quarter wave-plates, respectively.

Figure 2 Phase structure function averaged over 3000 separate phase structure functions. The 3000 phase structure functions were calculated from the wrapped phases determined from 3000 sets of sine and cosine interferograms.

Figure 3 Point-spread-functions for the uncorrected and correct probe beams after propagation through the phase plates..

Figure 4 Absolute Strehl ratios averaged over 100 separate frames. The experimental data is represented by the black line and a fit to the data assuming a Kolmogorov turbulence spectrum is given by the gray line. The error bars denote the standard deviation of the Strehl ratios, over 100 images

Figure 5 Phase structure function averaged over 3000 measured functions, which were calculated by unwrapping the wrapped phases determined from 3000 sets of sine and cosine interferograms

Figure 6 Point-spread-functions for the uncorrected and correct probe beams after propagation through the atmosphere.

Figure 7 Absolute Strehl ratios as a function of time. The solid black line represents the Strehl ratio with the AO system turned on, while the dashed black line represents the Strehl ratio with the system turned off. The solid gray line represents the Strehl ratio with the system turned off but with the center of mass of the point spread function moved to the central axis, as would occur if a tip/tilt system were running.

FIGURES

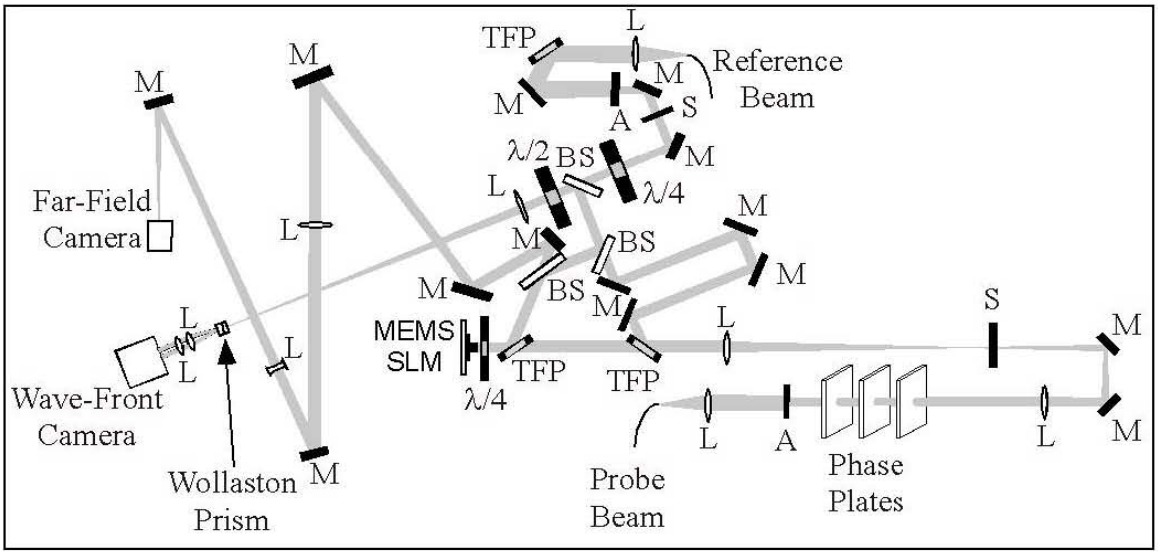

Figure 1

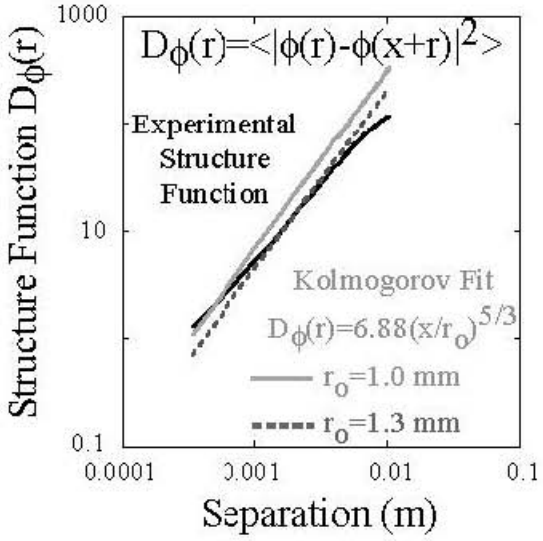
1000
10
0.1
0.0001
0.001
0.01
0.1
Structure Function $D_\phi(r)$
Separation (m)
$D_\phi(r)=<|\phi(r)-\phi(x+r)|^2>$
Experimental
Structure
Function
Kolmogorov Fit
$D_\phi(r)=6.88(x/r_o)^{5/3}$
r_o=1.0 mm
r_o=1.3 mm

Figure 2

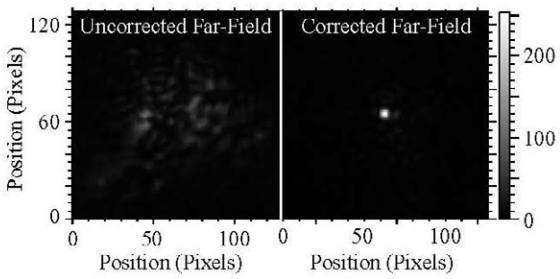
Uncorrected Far-Field
Corrected Far-Field
Position (Pixels)
Position (Pixels)
Position (Pixels)
120
60
0
0
50
100
0
50
100
200
100
0

Figure 3

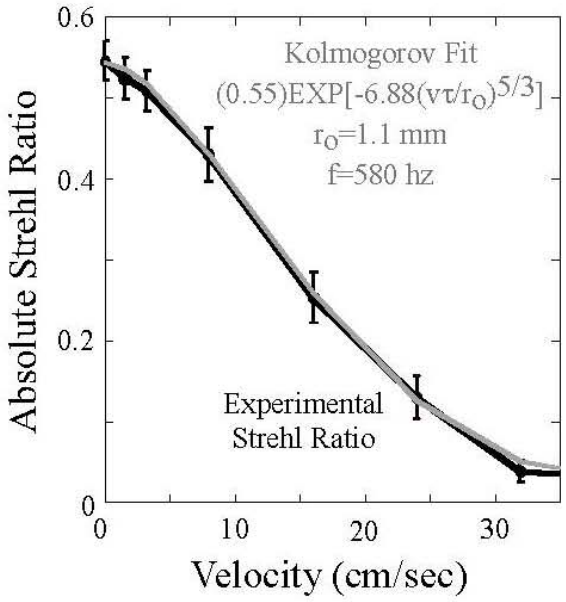
Kolmogorov Fit
(0.55)EXP[-6.88(vτ/r0)5/3]
r0=1.1 mm
f=580 hz
Experimental
Strehl Ratio
Absolute Strehl Ratio
Velocity (cm/sec)
0.6
0.4
0.2
0
0
10
20
30

Figure 4

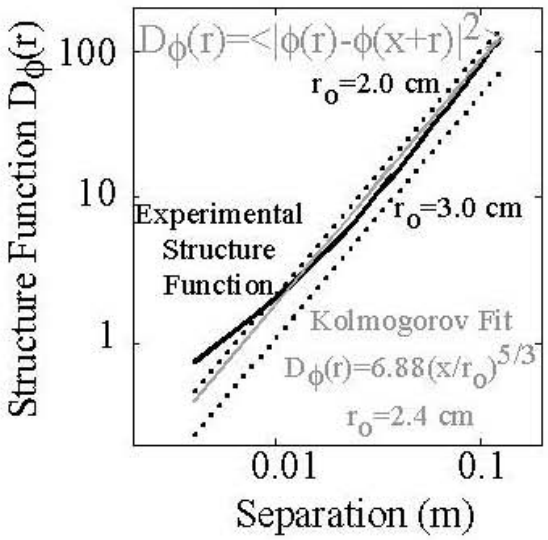
$D_\phi(r)=\langle|\phi(r)-\phi(x+r)|^2\rangle$
r_o=2.0 cm
r_o=3.0 cm
Experimental
Structure
Function
Kolmogorov Fit
$D_\phi(r)=6.88(x/r_o)^{5/3}$
r_o=2.4 cm
Structure Function $D_\phi(r)$
100
10
1
0.01
0.1
Separation (m)

Figure 5

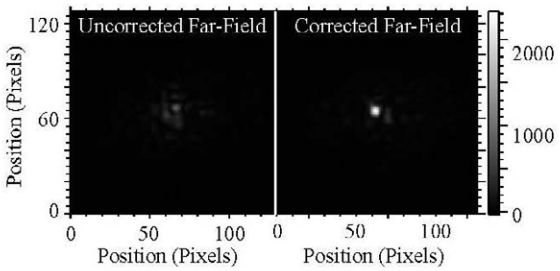
Uncorrected Far-Field
Corrected Far-Field
120
60
0
Position (Pixels)
0
50
100
Position (Pixels)
2000
1000
0

Figure 6

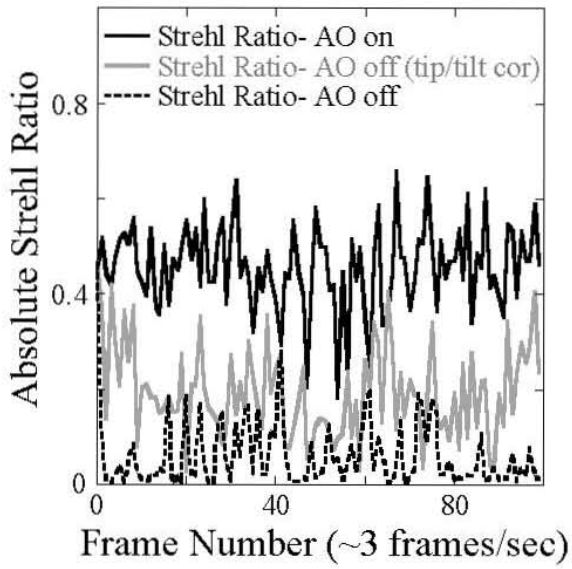
Strehl Ratio- AO on
Strehl Ratio- AO off (tip/tilt cor)
Strehl Ratio- AO off
Absolute Strehl Ratio
0.8
0.4
0
0
40
80
Frame Number (~3 frames/sec)

Figure 7

University of California
Lawrence Livermore National Laboratory
Technical Information Department
Livermore, CA 94551